Novel patient missense mutations in the HSD17B10 gene affect dehydrogenase and mitochondrial tRNA modification functions of the encoded protein

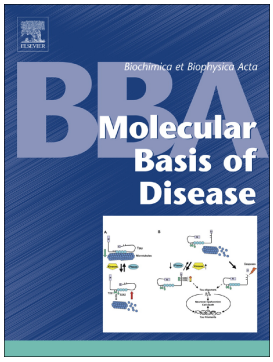

Stephanie Oerum, Martine Roovers, Michael Leichsenring, Cécile Acquaviva-Bourdain, Frauke Beermann, Corinne Gemperle-Britschgi, Alain Fouilhoux, Anne Korwitz-Reichelt, Henry J. Bailey, Louis Droogmans, Udo Oppermann, Jörn Oliver Sass, Wyatt W. Yue

PII: S0925-4439(17)30317-4
DOI: doi: 10.1016/j.bbadis.2017.09.002
Reference: BBADIS 64885

To appear in:

Received date: 15 February 2017
Revised date: 16 August 2017
Accepted date: 5 September 2017

Please cite this article as: Stephanie Oerum, Martine Roovers, Michael Leichsenring, Cécile Acquaviva-Bourdain, Frauke Beermann, Corinne Gemperle-Britschgi, Alain Fouilhoux, Anne Korwitz-Reichelt, Henry J. Bailey, Louis Droogmans, Udo Oppermann, Jörn Oliver Sass, Wyatt W. Yue , Novel patient missense mutations in the HSD17B10 gene affect dehydrogenase and mitochondrial tRNA modification functions of the encoded protein, (2017), doi: 10.1016/j.bbadis.2017.09.002

Novel patient missense mutations in the *HSD17B10* gene affect dehydrogenase and mitochondrial tRNA modification functions of the encoded protein

Stephanie Oerum[a], Martine Roovers[b], Michael Leichsenring[c], Cécile Acquaviva-Bourdain[d], Frauke Beermann[e], Corinne Gemperle-Britschgi[f], Alain Fouilhoux[g], Anne Korwitz-Reichelt[h], Henry J. Bailey[a], Louis Droogmans[i], Udo Oppermann[a,j], Jörn Oliver Sass*[e,f,h], Wyatt W. Yue*[a]

[a]Structural Genomics Consortium, Nuffield Department of Clinical Medicine, University of Oxford, Old Road Campus, Roosevelt Drive, OX3 7DQ Oxford, UK.

[b]Institut de Recherches Microbiologiques Jean-Marie Wiame, Bruxelles, Belgium.

[c]Department for Children and Adolescent Medicine, Ulm University Medical School, Ulm, Germany.

[d]Groupement Hospitalier Est, Centre de Biologie Est, Service Maladies Héréditaires du Métabolisme, Bron, France.

[e]University of Freiburg Children's Hospital, Laboratory of Clinical Biochemistry and Metabolism, Freiburg, Germany.

[f]University Children's Hospital and Children's Research Center, Clinical Chemistry & Biochemistry, Zürich, Switzerland.

[g]Centre de Référence des Maladies Héréditaires du Métabolisme, HCL, Bron France.

[h]Bonn-Rhein-Sieg University of Applied Sciences, Department of Natural Sciences, von-Liebig-Str. 20, 53359 Rheinbach, Germany.

[i]Laboratoire de Microbiologie, Universite libre de Bruxelles, Belgium.

[j]Botnar Research Centre, NIHR Oxford Biomedical Research Unit, Oxford, UK.

*To whom correspondence should be addressed. Tel: +44 (0) 1865 617757; Email: wyatt.yue@sgc.ox.ac.uk or Tel: +49 2241 865 9668; Email: joern.oliver.sass@h-brs.de.

ABSTRACT

MRPP2 (also known as HSD10/SDR5C1) is a multifunctional protein that harbours both catalytic and non-catalytic functions. The protein belongs to the short-chain dehydrogenase/reductases (SDR) family and is involved in the catabolism of isoleucine *in vivo* and steroid metabolism *in vitro*. MRPP2 also moonlights in a complex with the MRPP1 (also known as TRMT10C) protein for N1-methylation of purines at position 9 of mitochondrial tRNA, and in a complex with MRPP1 and MRPP3 (also known as PRORP) proteins for 5'-end processing of mitochondrial precursor tRNA. Inherited mutations in the *HSD17B10* gene encoding MRPP2 protein lead to a childhood disorder characterised by progressive neurodegeneration, cardiomyopathy or both. Here we report two patients with novel missense mutations in the *HSD17B10* gene (c.34G>C and c.526G>A), resulting in the p.V12L and p.V176M substitutions. Val12 and Val176 are highly conserved residues located at different regions of the MRPP2 structure. Recombinant mutant proteins were expressed and characterised biochemically to investigate their effects towards the functions of MRPP2 and associated complexes *in vitro*. Both mutant proteins showed significant reduction in the dehydrogenase, methyltransferase and tRNA processing activities compared to wildtype, associated with reduced stability for protein with p.V12L, whereas the protein carrying p.V176M showed impaired kinetics and complex formation. This study therefore identified two distinctive molecular mechanisms to explain the biochemical defects for the novel missense patient mutations.

Running title: Biochemical characterisation of two novel HSD10 mutations

Abbreviations: HSD10: 17β-hydroxysteroid dehydrogenase type 10, MRPP1: mitochondrial ribonuclease P protein subunit 1, MRPP2: mitochondrial ribonuclease P protein subunit 2, MRPP3: mitochondrial ribonuclease P protein subunit 3, SDR: short-chain dehydrogenase/reductases, L-methyl-3-HAD: L-2-methyl-3-hydroxyacyl-CoA dehydrogenase, MHBD: 2-methyl-3-hydroxybutyryl-CoA dehydrogenase, (mt)RNase P: mitochondrial RNase P, (mt)pre-tRNA: mitochondrial precursor tRNA, mitochondrial tRNAs: (mt)tRNA, m^1A9: 1-

methyladenosine at tRNA-position 9, m^1G9, 1-methylguanosine at tRNA-position 9, m^1R9: 1-methyladenosine/1-methylguanosine at tRNA-position 9.

Keywords: dehydrogenase, mitochondrial tRNA, HSD10, methyltransferase, tRNA processing, MRPP

1. INTRODUCTION

17β-hydroxysteroid dehydrogenase type 10 (HSD10; also known as mitochondrial ribonuclease P protein subunit 2, MRPP2, or short-chain dehydrogenase/reductase 5C1, SDR5C1) is a mitochondrial enzyme involved in multiple cellular pathways including fatty acid oxidation, amino acid degradation, steroid metabolism and mitochondrial tRNA maturation. HSD10/MRPP2 belongs to the family of NAD(P)(H)-dependent short-chain dehydrogenase/reductases (SDR) [1–3], and was first identified as the dehydrogenase enzyme L-2-methyl-3-hydroxyacyl-CoA dehydrogenase (L-methyl-3-HAD) that converts L-2-methyl-3-hydroxybutyryl-CoA to 2-methyl-acetoacetyl-CoA, the penultimate step of isoleucine metabolism by β-oxidation [4]. Since then, many *in vitro* SDR substrates have been identified for HSD10/MRPP2 including the sex hormone 17β-estradiol [5,6], bile acids [7], the neurosteroid allopregnanolone [8], and short straight-chain/branched-chain fatty acyl-CoA thioesters [9]. The protein is also known to be inhibited by amyloid-β peptide [10,11].

Missense mutations of the *HSD17B10* gene encoding HSD10/MRPP2 have been shown to cause an unusual neurodegenerative childhood disorder, 2-methyl-3-hydroxybutyryl-CoA dehydrogenase (MHBD) deficiency, more recently referred to as HSD10 disease [12]. Despite being reported only in a few patients, characterised by progressive neurodegeneration, cardiomyopathy or both, there is significant heterogeneity in the clinical manifestation [12]. A highly unusual feature of HSD10 disease that distinguishes this from other metabolic disorders is a lack of correlation between the clinical symptoms and the enzyme dehydrogenase activity, indicating a defect in other cellular pathway(s). To this end, several *HSD17B10* missense mutations lead to mitochondrial damage and apoptotic cell death [13], with defects in mitochondrial tRNA processing [14]. In line with this, HSD10/MRPP2 protein was identified to be an essential subunit of the mitochondrial RNase P ((mt)RNase P) complex responsible for processing of the 5'-end of mitochondrial precursor tRNAs ((mt)pre-tRNA), an important step in the maturation of mitochondrial RNAs [15]. HSD10 was hence assigned the alternative nomenclature of MRPP2, which will be used hereafter in the manuscript.

The (mt)RNase P complex, exclusively found in metazoans, consists of MRPP2 and two other nuclear-encoded proteins: MRPP1 (also known as TRMT10C, encoded by the *TRMT10C* gene)

and MRPP3 (also known as PRORP, encoded by the *KIAA0391* gene). MRPP1 belongs to the SPOUT family of RNA methyltransferases [16], whilst MRPP3 is a Mg^{2+}-dependent endoribonuclease containing the Nedd4-YacP nuclease (NYN) domain [17]. In addition to the RNase P activity of the ternary complex, MRPP1 and MRPP2 were found to form a binary subcomplex that methylates the N1-atom of purines at position 9 (m^1R9) in (mt)tRNAs [18]. The m^1A9 modification is shown to be crucial for the correct folding of human (mt)$tRNA^{Lys}$ [19,20].

To date, 13 missense patient mutations in MRPP2 have been reported (p.V65A, p.D86G, p.L122V, p.R130C, p.Q165H, p.A154T, p.A157V, p.A158V, p.P210S, p. K212E, p.R226Q, p.N247A, p.E249Q) [4,13,21–29]. Out of them, five have recently been characterised at the recombinant protein and biochemical levels [27,30]. Here we report two novel mutations identified in two families following Sanger sequencing, prompted by characteristic patterns of urine organic acids. The biochemical abnormalities of the mutated proteins were studied *in vitro* using expression, activity and binding assays. We show that the two novel mutations alter dehydrogenase activity and both tRNA modification activities (m^1R9 methylation and RNase P) of MRPP2 via different molecular mechanisms.

2. PATIENTS, MATERIALS AND METHODS

2.1 Patients

Family 1 (German):

The (male) index case first came to medical attention at age 13 months with an atonic seizure following two days of reduced dietary intake. Body temperature was at 38°C; the patient was fatigue and lips suggested cyanosis; blood glucose was elevated to 13.88 mmol/L(reference range 4.11 - 5.49 mmol/L), lactic acid to 8.9 mmol/L (reference range 0.5 – 2.2 mmol/L). Blood gas analysis revealed a pH of 7.373 (reference range 7.36 – 7.44), $pC0_2$ of 27.3 mmHg (reference range 35-45 mmHG) and a base excess of -12.1 mmol/L (reference range – 2 to +2 mmol/L). The major abnormality in metabolic investigations was an increase in urinary 2-methyl-3-hydroxybutyric acid (107 mmol/mol creatinine), in one investigation together with an elevated signal of tiglylglycine (91 mmol/mol creatinine; both compounds were determined within the panel of urinary organic acids and no official upper limits of the reference ranges exist, but both values were clearly considered elevated). This was accompanied by some increase of C5:1 acylcarnitine in the acylcarnitine pattern determined in dried blood spots (0.44 µmol/L; normal < 0.2 µmol/L). The combination of clinical observations and laboratory results prompted sequence analysis of the *HSD17B10* gene. The physical and neurological development of the patient was normal, although some subcortical impairment of myelinisation, and hyperintensities in paraventricular white matter had been noted at magnetic resonance tomography. The physical and neurological development remained normal during four years of follow-up.

The index case had two older brothers. The first brother (five years older than the index case, with no mutations in *HSD17B10* gene (see Results section)) presented with developmental impairment affecting cognition, speech development and motoric coordination. He showed growth hormone deficiency and a complex chromosomal rearrangement, but no increase in urinary 2-methyl-3-hydroxybutyric acid excretion. The second older brother (eight years older than the index case) was asymptomatic with normal physical and neurological development. For this brother, organic acids were determined in the urine and showed an increase in both 2-methyl-3-hydroxybutyric acid and tiglylglycine. During four years of follow-up, this boy showed

normal physical and neurological development. Magnetic resonance tomography of the neurocranium showed no abnormalities, except a small sella. The mother of the index case was asymptomatic. A paternal sample could not be obtained.

Family 2 (French):

The (female) patient presented at 12 months of age with breaking of her weight curve (-0.5 SD at 6 months of age, -2.5 SD at 12 months of age). Her height and brain circumference remained stable. She had hypotonia and was not able to sit. She further showed cerebellar ataxia, was developmentally delayed and did not speak. At 15 months of age, a systolic murmur appeared, compatible with asymptomatic dilated cardiomyopathy. At 18 months of age, a cardiac decompensation was observed which, despite treatment, let to the death of the patient at 21 months of age.

Urinary organic acid analysis showed elevated levels of 2-methyl-3-hydroxybutyric acid and tiglylglycine. Based on this profile, sequence analysis of the *HSD17B10* gene and enzyme activity testing were performed.

2.2 Mutation analysis and enzyme activity testing in patient samples

Genomic DNA was extracted from EDTA blood by standard methods. Exons 1 to 6 of the *HSD17B10* gene plus flanking intronic regions were analysed by Sanger sequencing. Assessment of the activity of L-2-methyl-3-hydroxybutyryl-CoA dehydrogenase activity in cell homogenates of fibroblasts and of lymphocytes, the latter immortalised by transformation with Epstein-Barr virus (EBV), was performed based on the description by Zschocke et al. 2000 [23].

2.3 Recombinant protein expression and purification

DNA fragments encoding human MRPP2 (MGC collection 2819721) or MRPP3 (MGC collection 5206545) were subcloned into pNIC28-Bsa4 vector (GenBank EF198106) incorporating an N-terminal His_6-tag. To generate an MRPP1-MRPP2 co-expression plasmid, a DNA fragment of human MRPP1 (MGC collection 4719195) and MRPP2, interspersed with a ribosome binding site, was subcloned into the pNIC28-Bsa vector. Constructs for MRPP2 carrying the patient missense mutations were generated by site-directed mutagenesis using the QuikChange kit (Agilent), based on the pNIC28-Bsa4 vector containing either full-length His_6-MRPP2 or both

mature His_6-MRPP1 and full-length MRPP2 in a bicistronic transcript. The presence of the DNA changes was verified by Sanger sequencing.

Plasmids were transformed into *E. coli* BL21(DE3)-R3-pRARE2 competent cells, cultured in Terrific Broth at 37°C, and induced with 0.1 mM isopropyl β-D-1-thiogalactopyranoside for overnight growth at 18°C. For small-scale expression and solubility tests, cell pellets from 50 mL cultures were lysed by sonication, fractionated by centrifugation, and the resulting lysate was applied to immobilised metal affinity column (IMAC) for protein purification.

For large-scale purification for biochemical assays, MRPP2 (wildtype and mutants), co-expressed MRPP1-MRPP2 complex, and MRPP3 cell pellets from 3-12 L cultures were lysed as described above, and recombinant proteins were purified by IMAC and size exclusion chromatography, treated with Tobacco Etch Virus protease overnight, and further purified by IMAC and ion-exchange chromatography with a NaCl-gradient.

2.4 Analytical size-exclusion chromatography (SEC)

MRPP2 wildtype or mutant protein at equal amounts were injected onto a Sepax SRT SEC-300 column (Sepax Technologies) pre-equilibrated in a buffer of 500 mM NaCl, 50 mM 4-(2-hydroxyethyl)-1-piperazineethanesulfonic acid (HEPES) pH 7.5, 5% glycerol, 0.5 mM tris(2-chloroethyl) phosphate (TCEP). Protein elution was detected as a UV absorbance peak. Five proteins of known molecular weight (MW) (Bio-Rad): thyroglobulin (bovine), γ-globulin (bovine), ovalbumin (chicken), myoglobin (horse) and vitamin B_{12}, were applied to the column under the same conditions as for the protein of interest for MW determination.

2.5 Differential Scanning Fluorimetry (DSF)

DSF was performed in a 96-well plate using an Mx3005p RT-PCR machine (Stratagene) with excitation and emission filters of 492 and 610 nm, respectively. Each well consisted of 2 µL protein in 2 µM DSF buffer (150 mM NaCl, 10 mM HEPES pH 7.5), 2 µL SYPRO ORANGE diluted 1000-fold in DSF buffer from the manufacturers stock (Invitrogen), and (if applicable) 2 µL ligand at various concentrations. Fluorescence intensities were measured from 25 to 96°C with a ramp rate of 3°C/min. Melting temperature (T_m) was determined by curve-fitting using

GraphPad Prism v.5.01 software, as described [31]. Data significance for DSF and other assays was evaluated using a standard P-test performed using the GraphPad Prism v.5.01 software.

2.6 SDR activity assay

100 µM NAD^+ and substrate (allopregnanolone or DL-3-hydroxybutyryl-CoA) of various concentrations (100 to 0.05 µM) were mixed in a buffer of 100 mM NaCl and 20 mM Tris-HCl pH 8.0, to a final volume of 50 µL, and dispensed to 384-well plates (Corning). 3.7 µM purified MRPP2 protein (wildtype or mutant) was added and the fluorescence from NAD^+ conversion to NADH was continuously measured at 350 nm excitation/450 nm emission in a PHERAstar FSX microplate reader (BMG LABTECH) for 30 min. The obtained fluorescence data were analysed with the MARS software (BMG LABTECH) and kinetic parameters (K_M, V_{max}) were obtained by fitting data to Michaelis-Menten equation. k_{cat} was calculated for four active sites of a MRPP2 tetramer.

2.7 In vitro transcription of mitochondrial tRNA precursors

cDNAs representing human mitochondrial $tRNA^{Ile}$ and $tRNA^{Val}$ precursors were designed with leader and trailer sequences of 30 and 15 nucleotides, respectively, and *in vitro* transcribed from a PCR-amplified template by T7 RNA polymerase using the Transcript Aid T7 High yield transcription kit (Thermo Scientific). The transcribed precursor tRNAs were purified using the RNeasy Mini Kit (Qiagen).

2.8 Methyltransferase activity assay

1 µCi [methyl-^{3}H]SAM (15 Ci/mmol) (PerkinElmer), 1 µM individual or complexed protein(s), and 1 µg *in vitro* transcribed (mt)pre-tRNA was diluted in a buffer of 50 mM Tris-HCl pH 8, 5 mM $MgCl_2$, 20 mM NaCl and 1 mM DTT to 200 µL. The solution was incubated for 60 min. at 37°C in a heat block. The reaction was stopped by phenol extraction and the (mt)pre-tRNA substrate was TCA-precipitated. Radioactive methylated (mt)pre-tRNA was captured on a filter and washed three times with ethanol prior to the measurement of radioactivity in a scintillation counter.

2.9 RNase P activity assay

RNase P cleavage was performed by mixing 300 nM MRPP1-MRPP2, 150 nM MRPP3, 10 units of ribonuclease inhibitors (RNasin from Promega) and 400 nM *in vitro* transcribed (mt)pre-tRNA^{Ile} in a buffer of 30 mM Tris-HCl pH 8, 40 mM NaCl, 4.5 mM $MgCl_2$ and 2 mM DTT, to a total reaction volume of 8.25 µL. The reaction was performed at room temperature and stopped after 30 minutes by transferring 1 µL of the reaction mixture into 5 µL 500 mM EDTA and heating to 95°C. This sample was analysed by denaturing-PAGE on a 6% TBE-urea gel (Invitrogen) run in TBE buffer (Invitrogen). The gel was stained for 30 min. with SYBRO GOLD (Invitrogen) diluted 1000-fold in TBE buffer from the manufactures stock, and imaged using the Bio-Rad ChemiDoc Imaging System.

2.10 Immunoblot analysis

Control and patient fibroblasts and EBV-transformed lymphocytes were homogenized by sonication in RIPA buffer (Sigma Aldrich) supplemented with protease inhibitors (Protease Inhibitor Cocktail, Sigma Aldrich). 30 µg of total protein were separated on 4-20% gradient gels (Biorad) and transferred to PVDF membranes. Membranes were blocked in 5% low-fat milk and probed with an MRPP2-specific antibody (1:500, abcam ab10260). Anti-α-Tubulin (1:1000, abcam ab7291) served as a loading control. SuperSignal West Femto Maximum Sensitivity Substrate (Thermo Fisher Scientific, 34095) and ECL (GE Healthcare, RPN2106) were used to detect chemiluminescence, respectively.

3. RESULTS

3.1 Mutation analysis and assessment of 2-methyl-3-hydroxybutyryl-coenzyme A dehydrogenase activity

Sequence analysis of the *HSD17B10* gene in the index case of family 1, yielded hemizygosity of the mutation c.526G>A in exon 5, predicted to result in a Val176-to-Met substitution (p.V176M). Prediction programs MutationTaster, PolyPhen-2 and SIFT consider this change as "disease causing", "probably damaging", and "damaging", respectively. The variant was neither found in ExAc nor in the 1000 G database. An enzyme activity assay for 2-methyl-3-hydroxybutyryl-CoA dehydrogenase, which was performed in lymphocytes transformed with Epstein-Barr virus, did not yield detectable enzyme activity. The mutation c.526G>A in the *HSD17B10* gene was also identified in the mother (heterozygote) and in the second brother (eight years older than the index case), who were both asymptomatic. In contrast, the first brother (five years older than the index case), that presented with major developmental impairment, did not have the *HSD17B10* mutation identified in his relatives.

In DNA of the patient of family 2, mutation analysis revealed the heterozygous mutation c.34G>C in exon 2 of the *HSD17B10* gene, which was not found in DNA of her parents and should result in replacement of Val12 by Leu (p.V12L). The p.V12L missense change is predicted to be "disease causing" by MutationTaster, "probably damaging" by PolyPhen-2, and "damaging" by SIFT servers. The mutation was neither found in ExAc nor in the 1000 G database. The 2-methyl-3-hydroxybutyryl-CoA dehydrogenase activity assay, which was performed in lymphocytes transformed with the Epstein-Barr virus, and in fibroblast homogenates, revealed major residual activities of 69% and 47%, respectively.

3.2 A structural annotation of known MRPP2 mutations

Residues Val12 and Val176 are highly conserved through evolution in the MRPP2 protein encoded by the *HSD17B10* gene. Including the two novel mutations reported here (p.V12L, p.V176M), there are in total 15 missense mutations reported for the HSD10 disease to date. MRPP2 forms a tetramer (dimer of dimers) with a Rossmann-fold as revealed by its crystal structure [32]. These missense mutations are distributed widely across each monomer of the

tetramer (Fig. 1A) with locations in core structural elements, in close proximity to catalytic residues, and at monomer-monomer interfaces. Val12 is located in the central β-sheet that forms the core structure of the Rossmann-fold (Fig. 1B). V176M is located in helix-αF which harbours two of the catalytic residues Tyr168 and Lys172 (Fig. 1C), and further residues involved in the proton-relay system as well as in substrate binding (Appendix, Fig. S1).

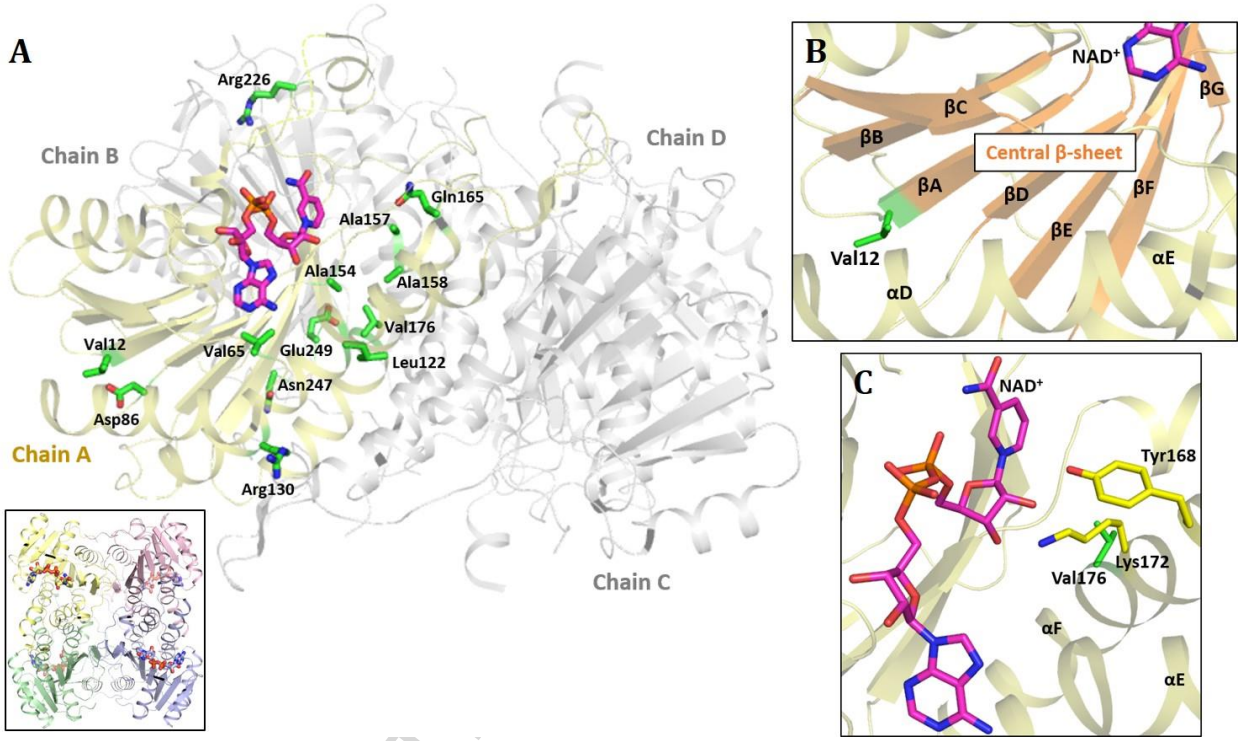

Fig. 1. Structural mapping of HSD10 disease mutations

(**A**) Sites of HSD10 patient missense mutations (green sticks) are mapped onto one monomer (yellow cartoon) of the MRPP2 tetramer (other subunits grey) (PDB: 2O23). The inset shows the architecture of the full MRPP2 tetramer. (**B**) Location of the p.V12L mutation (green stick) in the central β-sheet (orange). The secondary structure assignment is indicated for strands βA-G and helices αD-E. (**C**) Location of the p.V176M mutation. Catalytic residues (Lys172 and Tyr168) located in the same α-helical segment as the mutation site are shown as yellow sticks. NAD^+ cofactor is shown as purple sticks. Secondary structure assignment is indicated for helices αE-F.

3.3 Expression of MRPP2(V12L) and MRPP2(V176M)

To determine the effect of mutations towards the translated protein, recombinant MRPP2(WT), MRPP2(V12L) and MRPP2(V176M) were expressed in *E. coli*, and purified by affinity chromatography to compare expression and solubility levels. SDS-PAGE revealed similar levels of expression in *E. coli* for MRPP2 wildtype and mutant proteins (Fig. 2A and B), although the solubility of MRPP2(V12L) was significantly lower than that of MRPP2(WT) and MRPP2(V176M) (Fig. 2A and C). The purified recombinant proteins (Appendix, Fig. S2) were subjected to DSF to determine their thermostability (Fig. 2D). Consistent with the reduced solubility for MRPP2(V12L), the isolated protein (melting temperature (T_m) = 39.15±0.26) was found to be less thermostable than wildtype (T_m = 43.30±0.32), while MRPP2(V176M) (T_m = 48.93±0.10), by contrast, was more thermostable. In high-resolution analytical SEC, both MRPP2(V12L) and MRPP2(V176M) revealed the presence of an elution peak, like wildtype, that corresponds in MW to a tetramer (Appendix, Fig. S3). MRPP2(V12L) revealed a peak at the void volume indicative of protein aggregation, and is consistent with the observed lowered solubility. To further investigate if the reduced solubility and thermostability for p.V12L *in vitro* have any relevance in cells, we performed immunoblot analysis of patient fibroblasts and EBV-transformed lymphocytes harbouring this mutation, and showed that the level of MRPP2 protein detected in cell lysates were reduced compared to wildtype cells (Fig. 2F). We therefore concluded that the p.V12L affected the availability of functional protein *in vitro* and *in vivo*.

Next, binding of the cofactor substrate (NAD^+) and product (NADH) was assessed for recombinant wildtype and mutant proteins using DSF (Fig. 2E). NAD^+ and NADH increased the T_m of as-purified MRPP2(WT) by 3.42±0.12°C and 13.48±0.09°C, respectively. The T_m increases of MRPP2(V12L) towards NAD^+ and NADH are similar to the respective levels of MRPP2(WT). MRPP2(V176M), however, displayed much smaller T_m changes with NAD^+/NADH. Altogether, our data suggest that MRPP2(V176M), but not MRPP2(V12L), has altered its binding response to the cofactor ligands in the active site.

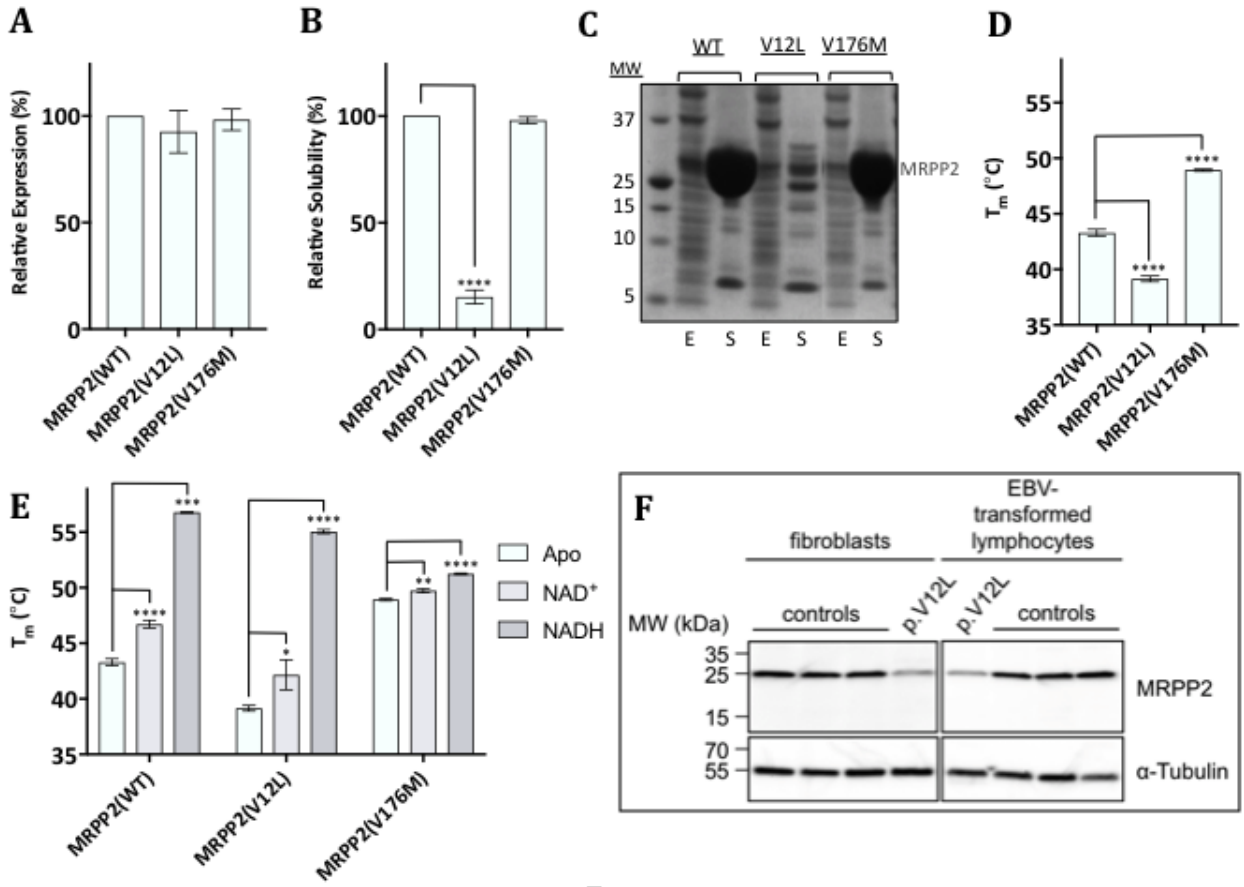

Fig. 2. Effect of p.V12L/p.V176M mutations on recombinant MRPP2 protein

(**A**) Intensities of SDS-PAGE bands from total lysate (S) samples of initial IMAC. (**B**) Intensities of SDS-PAGE bands from elution (E) fractions of initial IMAC. Wildtype (WT) is taken as 100%. (**C**) SDS-PAGE of the initial IMAC from which intensities for (A) and (B) were calculated. (**D**) Melting temperature (T_m) values for MRPP2 mutant proteins in the as-purified state. (**E**) T_m of MRPP2 proteins upon addition of NAD^+ or NADH. (**F**) Immunoblot analysis of control and patient fibroblasts and EBV-transformed lymphocytes. All samples were run on the same gel but different exposure times were applied. Standard deviations were determined from experiments n=3 for A and B, and n=4 for D and E. **=P<0.01, ***=P<0.001, ****=P<0.0001.

3.4 Dehydrogenase activity of MRPP2 mutants

We next monitored substrate binding and turnover of purified MRPP2 recombinant proteins (Appendix, Fig. S2), using two substrates that reflect the involvement of MRPP2 in fatty acid metabolism and neurosteroid conversion. For fatty acid metabolism, the substrate DL-3-hydroxybutyryl-CoA, a short straight-chain 3-hydroxyacyl-CoA thioester previously shown to be

turned over by MRPP2 *in vitro* using NAD^+ [10], was used. For steroid metabolism, we studied the NAD^+-dependent conversion of the neurosteroid allopregnanolone to 5α-dihydroprogesterone (5α-DHP).

To assay substrate binding to MRPP2, we employed DSF as before. For the substrate DL-3-hydroxybutyryl-CoA, binding was observed for wildtype and both mutant proteins (Fig. 3A), based on T_m increases upon adding substrate to the apoenzyme. However, the further increase in stability when both substrate and NAD^+ were present, compared to substrate alone, was clearly observed for wildtype and MRPP2(V12L), but much less so for MRPP2(V176M). For the allopregnanolone substrate, T_m increases (compared to apoenzyme) were also observed for all three proteins in the presence of substrate alone and when both substrate and NAD^+ were present (Fig. 3A), similar to what was observed for the CoA substrate. However, again there was little to no increase in stability for MRPP2(V176M) when both substrate and NAD^+ were present, compared to substrate alone, in contrast to wildtype and MRPP(V12L). Together our data suggest a poorer binding response of MRPP(V176M) towards both substrate and cofactor within the active site, compared to wildtype.

To assay substrate turnover, the dehydrogenase activity was tested for purified MRPP2(WT), MRPP2(V12L) and MRPP2(V176M) using the substrates used in in DSF (Table 1). All proteins were active towards DL-3-hydroxybutyryl-CoA with similar k_{cat} values, although the K_M of MRPP2(V176M) was increased 3-fold leading to an overall 3-fold reduction in catalytic efficiency (k_{cat}/K_M), compared to wildtype (Fig. 3B). For allopregnanolone, MRPP2(V12L) exhibited a nearly 3-fold decrease in catalytic efficiency compared to wildtype, due to both k_{cat} and K_M effects (Fig. 3C), while, surprisingly, MRPP2(V176M) did not turn over this substrate.

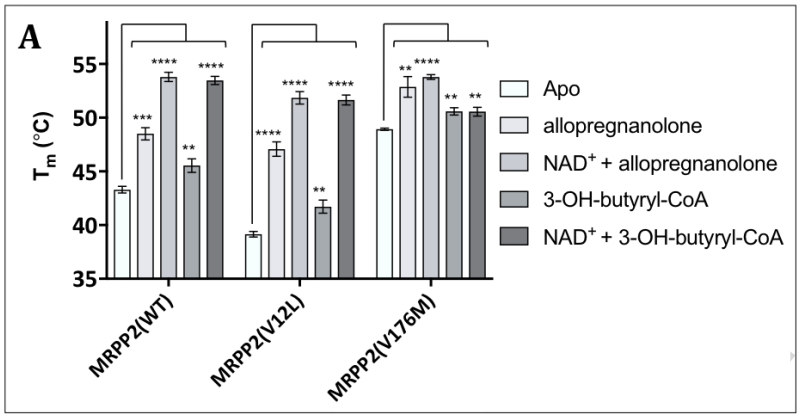

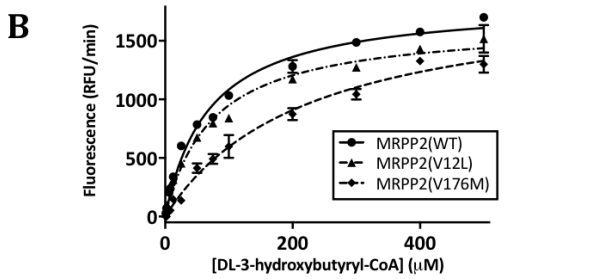

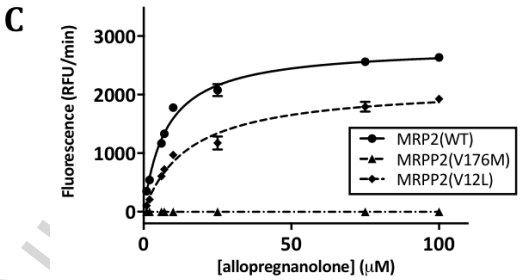

	MRPP2(WT)	MRPP2(V12L)	MRPP2(V176M)
k_{cat} (min^{-1})	458±17	412±18	481±29
K_M (μM)	69±8.3	74±10	223±30
k_{cat}/K_M ($min^{-1}\mu M^{-1}$)	6.6±0.13	5.6±0.15	2.2±0.15
V_{max} (μM·min^{-1})	1832±67	1649±72	1923±116

	MRPP2(WT)	MRPP2(V12L)	MRPP2(V176M)
k_{cat} (min^{-1})	706±13	540±19	-
K_M (μM)	7.7±0.45	15±1.6	N.D.
k_{cat}/K_M ($min^{-1}\mu M^{-1}$)	91±0.06	35±0.11	-
V_{max} (μM·min^{-1})	2824±52	2159±77	N.D.

Fig. 3. Effect of p.V12L/p.V176M mutations on MRPP2 dehydrogenase activity

(**A**) T_m of MRPP2 proteins upon addition of allopregnanolone and DL-3-hydroxybutyryl-CoA (3-OH-bytyryl-CoA) alone or with NAD^+. Michaelis-Menten plot for the catalysis of (**B**) (DL)-3-hydroxybutyryl-CoA and (**C**) allopregnanolone by MRPP2 wildtype and mutant proteins in the presence of NAD^+. RFU: relative fluorescence units. Kinetic parameters for the two reactions are shown on the right. N.D.: not determined. Standard deviations were determined from experiments n=3 for A-C.

3.5 Complex assembly with MRPP1

In addition to its dehydrogenase activity alone, MRPP2 is an essential subunit of the (mt)tRNA modification complexes of MRPP1-MRPP2 for purine-9 N1-methyltransferase (m^1R9) activity, and MRPP1-MRPP2-MRPP3 for 5'-end endonuclease (RNase P) activity. To determine the effect of p.V12L and p.V176M mutations towards these complexes and their associated activities, we first co-expressed each of MRPP2(WT), MRPP2(V12L) and MRPP2(V176M) with His_6-tagged MRPP1, and isolated the binary complexes by IMAC. In this one-step affinity purification, His_6-tagged MRPP1 pulled down similar amounts of untagged MRPP2(WT), MRPP2(V12L) and

MRPP2(V176M) (Appendix, Fig. S4), suggesting that the mutant proteins retained the ability to form a complex with MRPP1.

To determine the relative stability of the binary complexes, equal amounts of the MRPP1-MRPP2(WT/V12L/V176M) complexes that were isolated and partially purified by the initial IMAC step were incubated overnight and loaded onto a Superose 6 size exclusion column (Fig. 4A). In the chromatography profile, the ratio of MRPP1-complexed MRPP2 *vs.* uncomplexed MRPP2 is similar for MRPP2(WT) and MRPP2(V12L). Nevertheless, this ratio is shifted by a third towards uncomplexed protein for MRPP2(V176M), indicating a higher tendency for the isolated MRPP1-MRPP2(V176M) complex to dissociate over time, compared to MRPP1-MRPP2(WT) and MRPP1-MRPP2(V12L). The destabilised MRPP1-MRPP2(V176M) complex was further disintegrated in the subsequent anion exchange chromatography step, while the complexes containing MRPP2(WT) and MRPP2(V12L) stayed intact (data not shown). Together our data indicates a more transient nature of the MRPP1-MRPP2(V176M) complex compared to MRPP1-MRPP2(WT) and MRPP1-MRPP2(V12L), resulting in a higher tendency to dissociate.

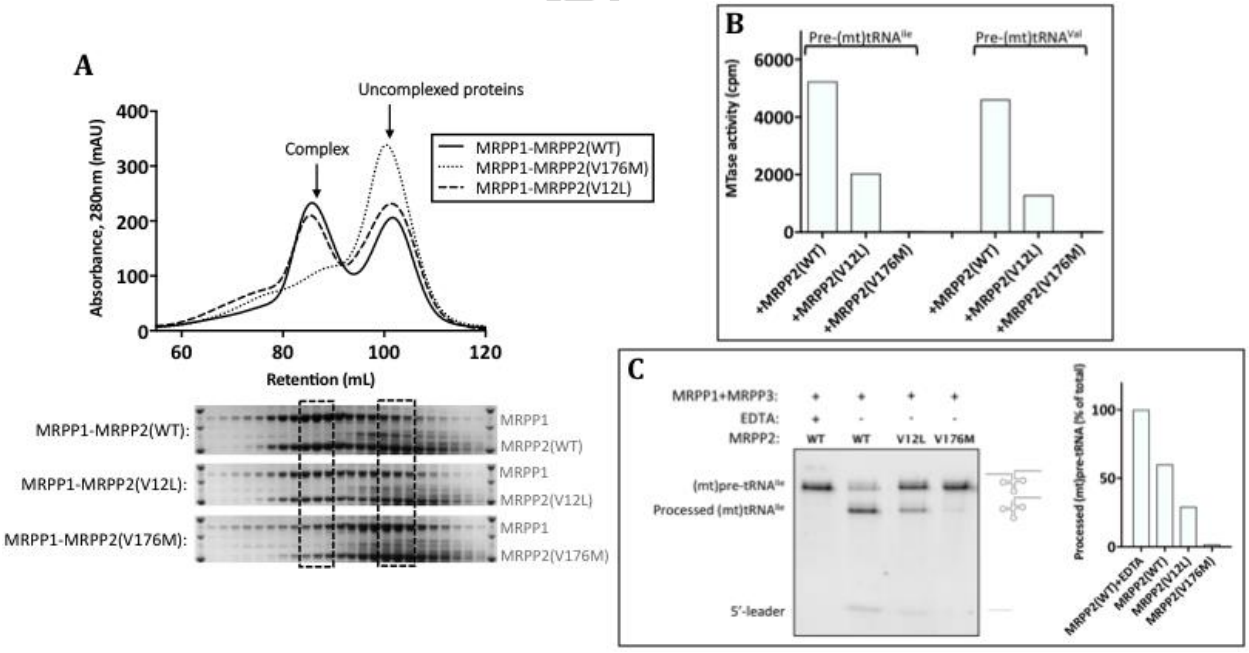

Fig. 4. Effect of p.V12L/p.V176M mutations on tRNA processing functions of MRPP2-associated complexes (**A**) Size exclusion chromatography profile of MRPP1 co-expressed with MRPP2(WT/V12L/V176M). The dashed boxes indicate the fractions from the chromatogram (top) and SDS-PAGE (bottom) where proteins form a complex, or are present as separate species in solution. (**B**)

m^1G9 and m^1A9 methyltransferase activity of the MRPP1-MRPP2(WT/V12L/V176M) complexes. (**C**) RNase P activity towards mitochondrial (mt)pre-$tRNA^{Ile}$ of the MRPP complex that contains MRPP2(WT/V12L/V176M), measured by change in electrophoretic mobility between precursor and processed (mt)tRNA. For B and C, values shown are mean average from n=2.

3.6 tRNA-dependent methyltransferase and endonuclease activities

The MRPP1-MRPP2(WT/V12L/V176M) complexes were next assayed for the m^1R9 methyltransferase activity towards (mt)tRNAs (Fig. 4B, Table 1) containing either guanine (G) or adenine (A) at position 9, for formation of m^1G9 or m^1A9, respectively. The m^1G9 methyltransferase activity was tested with *in vitro* transcribed (mt)pre-$tRNA^{Ile}$ as substrate, and m^1A9 activity with (mt)pre-$tRNA^{Val}$. MRPP1-MRPP2(V12L) showed a 2.5-fold reduction of m^1G9 methyltransferase activity and a 3.5-fold reduction in m^1A9 methyltransferase activity, compared to the wildtype complex. For MRPP1-MRPP2(V176M), almost no methyltransferase activity was observed for either m^1G9 or m^1A9 formation.

The RNase P activity towards the 5'-end of (mt)pre-tRNA was carried out by incubating the MRPP1-MRPP2(WT/V12L/V176M) complexes with purified MRPP3 (Appendix, Fig. S2), in the presence of Mg^{2+} (required for the cleavage reaction) and *in vitro* transcribed (mt)pre-$tRNA^{Ile}$ substrate (Fig. 4C, left). In this assay, 60±1% of (mt)pre-$tRNA^{Ile}$ was processed by MRPP1-MRPP2(WT)-MRPP3, compared to 29±6% (2-fold decrease) for MRPP1-MRPP2(V12L)-MRPP3 and only 1.9±0.2% (> 30-fold decrease) for MRPP1-MRPP2(V176M)-MRPP3 (Fig. 4C, right) (Table 1). The fold decrease of RNase P activity for the mutant ternary complexes is comparable to their identified methyltransferase activities.

4. DISCUSSION

MRPP2 is a multifunctional protein harbouring both SDR and non-SDR functions. As an SDR, MRPP2 acts on many substrates, amongst others isoleucine, sex steroids, bile acids and neurosteroids. In its non-SDR function, MRPP2 moonlights in binary and ternary protein-complexes involved in tRNA modifications. Several missense mutations are reported in the *HSD17B10* gene coding for MRPP2, and for some mutations the phenotype severity does not correlate with residual SDR activity, drawing attention to the non-SDR functions of MRPP2. In this work, two novel mutations in MRPP2 (pV12L and p.V176M) have been identified, and characterised *in vitro*. On the whole (Table 1), both p.V12L and p.V176M mutations reduced the dehydrogenase activity of MRPP2, m^1R9 methyltransferase activity of MRPP1-MRPP2 and RNase P activity of MRPP1-MRPP2-MRPP3, albeit in varying degrees and seemingly via different molecular defects to MRPP2 protein properties.

	Dehydrogenase act. [$min^{-1}\mu M^{-1}$] (k_{cat}/K_M)		**Methyltransferase act.** [cpm]		**RNase P act.** [% of total (mt)pre-tRNA]	**Complex stability**	**Structure location**
	CoA thioester	**Steroid**	**Adenine**	**Guanine**			
WT	6.6±0.13	91±0.06	4609±819	5238±394	60±1	Stable	
p.V12L	5.6±0.15	35±0.11	1258±49	2036±85	29±6	Stable	β-sheet
p.V176M	2.2±0.15	-	26±31	35±31	2±0.2	Unstable	Helix αE

Table 1. Outline of the residual activities measured in this report, along with the structural location and ability to form the binary complex (given as stable: complex formed, or unstable: complex dissociating) for the two novel mutations identified in MRPP2 (p.V12L and p.V176M).

We propose that the p.V12L missense mutation results in a less thermostable MRPP2 protein, reducing protein abundance both in recombinant expression and in patient fibroblasts and EBV-transformed lymphocytes, an effect that indirectly impacts on the associated enzyme functions. Val12 is situated at the beginning of strand-βA that forms part of the core Rossmann-fold β-sheet. When mutated to Leu, this residue likely creates a steric clash with the nearby Arg84 main-chain and Phe82 side-chain atoms, towards the end of the helix-αC (Appendix, Fig. S5A). The steric constraints could imply a rearrangement of the implicated residues that destabilise

the core β-sheet and overall structure. Such destabilisation can explain the significantly lowered solubility of MRPP2(V12L) and increased tendency to aggregate compared to wildtype, although once isolated, the soluble mutant protein exhibits only a moderately reduced SDR activity and retained the ability to bind both substrates and cofactors. Protein destabilisation would also affect the tRNA processing functions of MRPP2 by reducing the level of soluble mutant protein for complex formation.

We propose that the p.V176M mutation disrupts MRPP2 functions by a mechanism different from p.V12L. Val176 is located in helix-αF that contributes to one side of the substrate-binding pocket (Fig. 1C). Helix-αF is immediately followed by a loop-helix-loop segment that contains many catalytically important residues, including Gln162 and Gln165 implicated in ligand binding [33,34], Ser155 from the catalytic tetrad [35], residues involved in formation of the proton-relay system [35–37], and Ala154 and Thr153 from the cofactor binding pocket [38]. Mutation of Val176-to-Met could cause steric clashes with this loop-helix-loop segment, *i.e.* side-chains of Ala156 and the Phe159, altering positions of the catalytically important residues that result in k_{cat} and K_M changes to catalysis (Appendix, Fig. S5B), and lowered T_m response in the presence of substrate and cofactor at the active site, compared to wildtype. Altogether, this supports the more pronounced effect on MRPP2 functions (dehydrogenase, methyltransferase, RNase P activities) for p.V176M, compared to p.V12L.

An inhibitory effect of both mutations on the dehydrogenase activity of MRPP2 was not only observed with purified proteins for the substrates 3-hydroxybutyryl-CoA and allopregnanolone, but also in a comparable manner with patient cells and 2-methyl-3-hydroxybutyryl-CoA. However, the higher residual activity in the cells of the patient from family 2, compared with the residual activity found for the patient from family 1, may indicate a lower severity of the *de novo* mutation p.V12L in family 2, compared with p.V176M in family 1, but may also be due to heterozygosity and/or X-inactivation (family 2) in contrast to hemizygosity (index case, family 1). In agreement with previous observations made (family of case 2 that was described in the supporting information of [13]), clinical features in family 1 did not segregate with the mutation in the *HSD17B10* gene. Thus, the mutation p.V176M cannot be considered causative for the clinical features observed in family members of the index case in family 1. For family 2, the

clinical course of the female index case resembled that of patients suffering from what is considered the “classical” presentation of the infantile form of HSD10 disease [12]. This clinical phenotype has so far only been reported for affected boys (for review, see [12]), but is not unexpected to occur in female patients, in view of random X-inactivation of the *HSD17B10* gene [26].

In our activity assay, MRPP2(V176M) showed an increased K_M-value indicative of poor substrate accommodation, possibly due to an altered active site. These alterations seem to affect the steroid substrate more than the DL-3-hydroxybutyryl-CoA, as shown for MRPP2(V176M). One reason for this could be the smaller molecular size of allopregnanolone (318.49 Da) compared to DL-3-hydroxybutyryl-CoA (853.63 Da). The smaller steroid would have fewer interaction points with the protein active site, compared to the larger CoA thioester substrate. Small changes to the pocket could therefore impact more severely the binding of allopregnanolone, compared to DL-3-hydroxybutyryl-CoA, which might be compensated by additional interaction points outside the immediate active site pocket. Consistent with this hypothesis, our DSF data indeed showed smaller T_m increases upon adding substrate (substrate with NAD^+) to the MRPP2(V176M) apoenzyme for DL-3-hydroxybutyryl-CoA, than for allopregnanolone (Fig. 3A). The p.V176M mutation also caused MRPP2 to dissociate from the complex with MRPP1 more readily than wildtype, which could explain the nearly abolished m^1R9 methyltransferase and RNase P activities observed, as both of these activities require an intact complex [18]. Further structural analysis is required to elucidate how this mutation disturbs MRPP1-MRPP2 interaction, since Val176 is not surface exposed and therefore not in a location predicted to be the protein-protein interface.

ACKNOWLEDGMENTS

Technical assistance by Annegret Flier and financial support by Fondation Claude et Giuliana and Olga Mayenfisch-Stiftung is gratefully acknowledged. We thank the Metabolic Laboratory, Center for Metabolic Diseases, University Hospital Heidelberg (Germany), for the determination of metabolites in samples of family 1.

FUNDING

This work was funded by the Structural Genomics Consortium, which is a registered charity (number 1097737) that receives funds from AbbVie, Boehringer Ingelheim, the Canada Foundation for Innovation, the Canadian Institutes for Health Research, Genome Canada, GlaxoSmithKline, Janssen, Lilly Canada, the Novartis Research Foundation, the Ontario Ministry of Economic Development and Innovation, Pfizer, Takeda, and the Wellcome Trust (092809/Z/10/Z). The project was also supported by the "Startförderung 2016" of the Bonn-Rhein-Sieg-University of Applied Sciences to J.O.S.

DISCLOSURE STATEMENT

No potential conflicts of interest are reported for any of the authors.

REFERENCES

[1] H. Jörnvall, B. Persson, M. Krook, S. Atrian, R. Gonzàlez-Duarte, J. Jeffery, D. Ghosh, Short-chain dehydrogenases/reductases (SDR), Biochemistry. 34 (1995) 6003–6013.

[2] Y. Kallberg, U. Oppermann, H. Jörnvall, B. Persson, Short-chain dehydrogenase/reductase (SDR) relationships : A large family with eight clusters common to human, animal, and plant genomes, Protein Sci. 11 (2002) 636–641. doi:10.1110/ps.26902.spite.

[3] K.L. Kavanagh, H. Jörnvall, B. Persson, U. Oppermann, Medium- and short-chain dehydrogenase/reductase gene and protein families : the SDR superfamily: functional and structural diversity within a family of metabolic and regulatory enzymes., Cell. Mol. Life Sci. 65 (2008) 3895–906. doi:10.1007/s00018-008-8588-y.

[4] S.-Y. Yang, X.-Y. He, S.E. Olpin, V.R. Sutton, J. McMenamin, M. Philipp, R.B. Denman, M. Malik, Mental retardation linked to mutations in the HSD17B10 gene interfering with neurosteroid and isoleucine metabolism, Proc. Natl. Acad. Sci. U. S. A. 106 (2009) 14820–4. doi:10.1073/pnas.0902377106.

[5] X. He, G. Merz, P. Mehta, H. Schulz, S. Yang, Human brain short chain l-3-hydroxyacyl coenzyme A dehydrogenase is a single-domain multifunctional enzyme: characterization of a novel 17 β-hydroxysteroid dehydrogenase, J. Biol. Chem. 274 (1999) 15014–15019.

[6] X. He, Y. Yang, H. Schulz, S. Yang, Intrinsic alcohol dehydrogenase and hydroxysteroid dehydrogenase activities of human mitochondrial short-chain, 345 (2000) 139–143.

[7] N. Shafqat, H.-U. Marschall, C. Filling, E. Nordling, X.-Q. Wu, L. Björk, J. Thyberg, E. Mårtensson, S. Salim, H. Jörnvall, U. Oppermann, Expanded substrate screenings of human and Drosophila type 10 17β-hydroxysteroid dehydrogenases (HSDs) reveal multiple specificities in bile acid and steroid hormone metabolism: characterization of multifunctional 3α/7α/7β/17β/20β/21-HSD, Biochem. J. 376 (2003) 49–60. doi:10.1042/BJ20030877.

[8] X.-Y. He, J. Wegiel, Y.-Z. Yang, R. Pullarkat, H. Schulz, S.-Y. Yang, Type 10 17beta-hydroxysteroid dehydrogenase catalyzing the oxidation of steroid modulators of γ-aminobutyric acid type A receptors, Mol. Cell. Endocrinol. 229 (2005) 111–7. doi:10.1016/j.mce.2004.08.011.

[9] M.J. Luo, L.-F. Mao, H. Schulz, Short-chain 3-Hydroxy-2-methylacyl-CoA Dehydrogenase from Rat Liver: Purification and Characterization of a Novel Enzyme of Isoleucine Metabolism, Biochem. Biophys. 321 (1995) 214–220.

[10] X. He, H. Schulz, S.-Y. Yang, A human brain l-3-hydroxyacyl-coenzyme A dehydrogenase is identical to an amyloid β-peptide-binding protein involved in Alzheimer's disease, J. Biol. Chem. 273 (1998) 10741–10746.

[11] U. Oppermann, S. Salim, L.O. Tjernberg, L. Terenius, H. Jörnvall, Binding of amyloid β-peptide to mitochondrial hydroxyacyl-CoA dehydrogenase (ERAB): Regulation of an SDR enzyme activity with implications for apoptosis in Alzheimer's disease, FEBS Lett. 451 (1999) 238–242. doi:10.1016/S0014-5793(99)00586-4.

[12] J. Zschocke, HSD10 disease: clinical consequences of mutations in the HSD17B10 gene., J. Inherit. Metab. Dis. 35 (2012) 81–9. doi:10.1007/s10545-011-9415-4.

[13] K. Rauschenberger, K. Schöler, J.O. Sass, S. Sauer, Z. Djuric, C. Rumig, N.I. Wolf, J.G. Okun, S. Kölker, H. Schwarz, C. Fischer, B. Grziwa, H. Runz, A. Nümann, N. Shafqat, K.L. Kavanagh, G. Hämmerling, R.J.A. Wanders, J.P.H. Shield, U. Wendel, D. Stern, P. Nawroth, G.F. Hoffmann, C.R. Bartram, B. Arnold, A. Bierhaus, U. Oppermann, H. Steinbeisser, J. Zschocke, A non-enzymatic function of 17β-hydroxysteroid dehydrogenase type 10 is required for mitochondrial integrity and cell survival, EMBO Mol. Med. 2 (2010) 51–62. doi:10.1002/emmm.200900055.

[14] A.J. Deutschmann, A. Amberger, C. Zavadil, H. Steinbeisser, J.A. Mayr, R.G. Feichtinger, S. Oerum, W.W. Yue, J. Zschocke, Mutation or knock-down of 17β-hydroxysteroid dehydrogenase type 10 cause loss of MRPP1 and impaired processing of mitochondrial heavy strand transcripts, Hum. Mol. Genet. 23 (2014) 3618–28. doi:10.1093/hmg/ddu072.

[15] J. Holzmann, P. Frank, E. Löffler, K.L. Bennett, C. Gerner, W. Rossmanith, RNase P without RNA: Identification and Functional Reconstitution of the Human Mitochondrial tRNA Processing Enzyme, Cell. 135 (2008) 462–474. doi:10.1016/j.cell.2008.09.013.

[16] V. Anantharaman, E. V Koonin, L. Aravind, SPOUT: a Class of Methyltransferases that Includes spoU and trmD RNA Methylase Superfamilies, and Novel Superfamilies of

Predicted Prokaryotic RNA methylases, J. Mol. Microbiol. Biotechnol. 4 (2002) 71–75.

[17] V. Anantharaman, L. Aravind, The NYN Domains Novel Predicted RNAses with a PIN Domain-Like Fold, RNA Biol. 3 (2006) 18–27.

[18] E. Vilardo, C. Nachbagauer, A. Buzet, A. Taschner, J. Holzmann, W. Rossmanith, A subcomplex of human mitochondrial RNase P is a bifunctional methyltransferase - extensive moonlighting in mitochondrial tRNA biogenesis, Nucleic Acids Res. 40 (2012) 11583–93. doi:10.1093/nar/gks910.

[19] M. Helm, H. Brulé, F. Degoul, C. Cepanec, J.-P. Leroux, R. Giegé, C. Florentz, The presence of modified nucleotides is required for cloverleaf folding of a human mitochondrial tRNA, Nucleic Acids Res. 26 (1998) 1636–1643. doi:10.1093/nar/26.7.1636.

[20] F. Voigts-Hoffmann, M. Hengesbach, A.Y. Kobitski, A. Van Aerschot, P. Herdewijn, G.U. Nienhaus, M. Helm, A Methyl Group Controls Conformational Equilibrium in Human Mitochondrial tRNALys, J. Am. Chem. Soc. 129 (2007) 13382–13383. doi:10.1021/ja075520+.

[21] L.H. Seaver, X.-Y. He, K. Abe, T. Cowan, G.M. Enns, L. Sweetman, M. Philipp, S. Lee, M. Malik, S.-Y. Yang, A novel mutation in the HSD17B10 gene of a 10-year-old boy with refractory epilepsy, choreoathetosis and learning disability., PLoS One. 6 (2011) e27348. doi:10.1371/journal.pone.0027348.

[22] R. Ofman, J.P.N. Ruiter, M. Feenstra, M. Duran, B.T. Poll-The, J. Zschocke, R. Ensenauer, W. Lehnert, J.O. Sass, W. Sperl, R.J.A. Wanders, 2-Methyl-3-hydroxybutyryl-CoA dehydrogenase deficiency is caused by mutations in the HADH2 gene., Am. J. Hum. Genet. 72 (2003) 1300–7. doi:10.1086/375116.

[23] J. Zschocke, J.P. Ruiter, J. Brand, M. Lindner, G.F. Hoffmann, R.J. Wanders, E. Mayatepek, Progressive infantile neurodegeneration caused by 2-methyl-3-hydroxybutyryl-CoA dehydrogenase deficiency: a novel inborn error of branched-chain fatty acid and isoleucine metabolism., Pediatr. Res. 48 (2000) 852–5. doi:10.1203/00006450-200012000-00025.

[24] T. Fukao, K. Akiba, M. Goto, N. Kuwayama, M. Morita, T. Hori, Y. Aoyama, R. Venkatesan, R. Wierenga, Y. Moriyama, T. Hashimoto, N. Usuda, K. Murayama, A. Ohtake, Y.

Hasegawa, Y. Shigematsu, Y. Hasegawa, The first case in Asia of 2-methyl-3-hydroxybutyryl-CoA dehydrogenase deficiency (HSD10 disease) with atypical presentation, J. Hum. Genet. 59 (2014) 609–614. doi:10.1038/jhg.2014.79.

[25] S. Akagawa, T. Fukao, Y. Akagawa, H. Sasai, U. Kohdera, M. Kino, Y. Shigematsu, Y. Aoyama, K. Kaneko, Japanese Male Siblings with 2-Methyl-3-Hydroxybutyryl- CoA Dehydrogenase Deficiency (HSD10 Disease) Without Neurological Regression, JIMD Rep. (2016) 113–116. doi:10.1007/8904.

[26] J. García-Villoria, A. Navarro-Sastre, C. Fons, C. Pérez-Cerdá, A. Baldellou, M.A. Fuentes-Castelló, I. González, A. Hernández-Gonzalez, C. Fernández, J. Campistol, C. Delpiccolo, N. Cortés, A. Messeguer, P. Briones, A. Ribes, Study of patients and carriers with 2-methyl-3-hydroxybutyryl-CoA dehydrogenase (MHBD) deficiency: difficulties in the diagnosis., Clin. Biochem. 42 (2009) 27–33. doi:10.1016/j.clinbiochem.2008.10.006.

[27] M.J. Falk, X. Gai, M. Shigematsu, E. Vilardo, R. Takase, E. McCormick, T. Christian, E. Place, E.A. Pierce, M. Consugar, H.B. Gamper, W. Rossmanith, Y.-M. Hou, A novel HSD17B10 mutation impairing the activities of the mitochondrial RNase P complex causes X-linked intractable epilepsy and neurodevelopmental regression, RNA Biol. 13 (2016) 477–485. doi:10.1080/15476286.2016.1159381.

[28] C. Perez-Cerda, J. García-Villoria, R. Ofman, P.R. Sala, B. Merinero, J. Ramos, M.T. García-Silva, B. Beseler, J. Dalmau, R.J.A. Wanders, M. Ugarte, A. Ribes, 2-Methyl-3-hydroxybutyryl-CoA dehydrogenase (MHBD) deficiency: an X-linked inborn error of isoleucine metabolism that may mimic a mitochondrial disease., Pediatr. Res. 58 (2005) 488–91. doi:10.1203/01.pdr.0000176916.94328.cd.

[29] C.F. Lorea, A. Sitta, R. Yamamoto, F.P.A. Paulo, P.F. Vairo, C.R.M. Rieder, M. Wajner, I.V.D. Schwartz, R. Giugliani, L.B. Jardim, J.O. Sass, J.A. Saute, Case report: atypical juvenile parkinsonism and basal ganglia calcifications due to HSD10 disease, Abstr. J Inherit Metab Dis. 38 (2015) 210.

[30] E. Vilardo, W. Rossmanith, Molecular insights into HSD10 disease: impact of SDR5C1 mutations on the human mitochondrial RNase P complex, Nucleic Acids Res. (2015) 1–9. doi:10.1093/nar/gkv408.

[31] F.H. Niesen, H. Berglund, M. Vedadi, The use of differential scanning fluorimetry to detect ligand interactions that promote protein stability, Nat. Protoc. 2 (2007) 2212–2221. doi:10.1038/nprot.2007.321.

[32] C.R. Kissinger, P.A. Rejto, L.A. Pelletier, J.A. Thomson, R.E. Showalter, M.A. Abreo, C.S. Agree, S. Margosiak, J.J. Meng, R.M. Aust, D. Vanderpool, B. Li, A. Tempczyk-Russell, J.E. Villafranca, Crystal Structure of Human ABAD/HSD10 with a Bound Inhibitor: Implications for Design of Alzheimer's Disease Therapeutics., J. Mol. Biol. 342 (2004) 943–52. doi:10.1016/j.jmb.2004.07.071.

[33] A.J. Powell, J.A. Read, M.J. Banfield, F. Gunn-Moore, S.D. Yan, J. Lustbader, A.R. Stern, D.M. Stern, R.L. Brady, Recognition of structurally diverse substrates by type II 3-hydroxyacyl-CoA dehydrogenase (HADH II)/Amyloid-β binding alcohol dehydrogenase (ABAD), J. Mol. Biol. 303 (2000) 311–327. doi:10.1006/jmbi.2000.4139.

[34] S.-Y. Yang, X.-Y. He, C. Isaacs, C. Dobkin, D. Miller, M. Philipp, Roles of 17β-hydroxysteroid dehydrogenase type 10 in neurodegenerative disorders, J. Steroid Biochem. Mol. Biol. 143 (2014) 460–472. doi:10.1016/j.jsbmb.2014.07.001.

[35] C. Filling, K.D. Berndt, J. Benach, S. Knapp, T. Prozorovski, E. Nordling, R. Ladenstein, H. Jörnvall, U. Oppermann, Critical residues for structure and catalysis in short-chain dehydrogenases/reductases., J. Biol. Chem. 277 (2002) 25677–84. doi:10.1074/jbc.M202160200.

[36] U.C. Oppermann, C. Filling, H. Jörnvall, Forms and functions of human SDR enzymes., Chem. Biol. Interact. 130–132 (2001) 699–705. http://www.ncbi.nlm.nih.gov/pubmed/11306087.

[37] R. Ladenstein, J.O. Winberg, J. Benach, Medium- and short-chain dehydrogenase/reductase gene and protein families: Structure-function relationships in short-chain alcohol dehydrogenases, Cell. Mol. Life Sci. 65 (2008) 3918–3935. doi:10.1007/s00018-008-8590-4.

[38] A.C. Wallace, R.A. Laskowski, J.M. Thornton, LIGPLOT: a program to generate schematic diagrams of protein-ligand interactions, Protein Eng. 8 (1995) 127–134. doi:10.1093/protein/8.2.127.

Graphical abstract

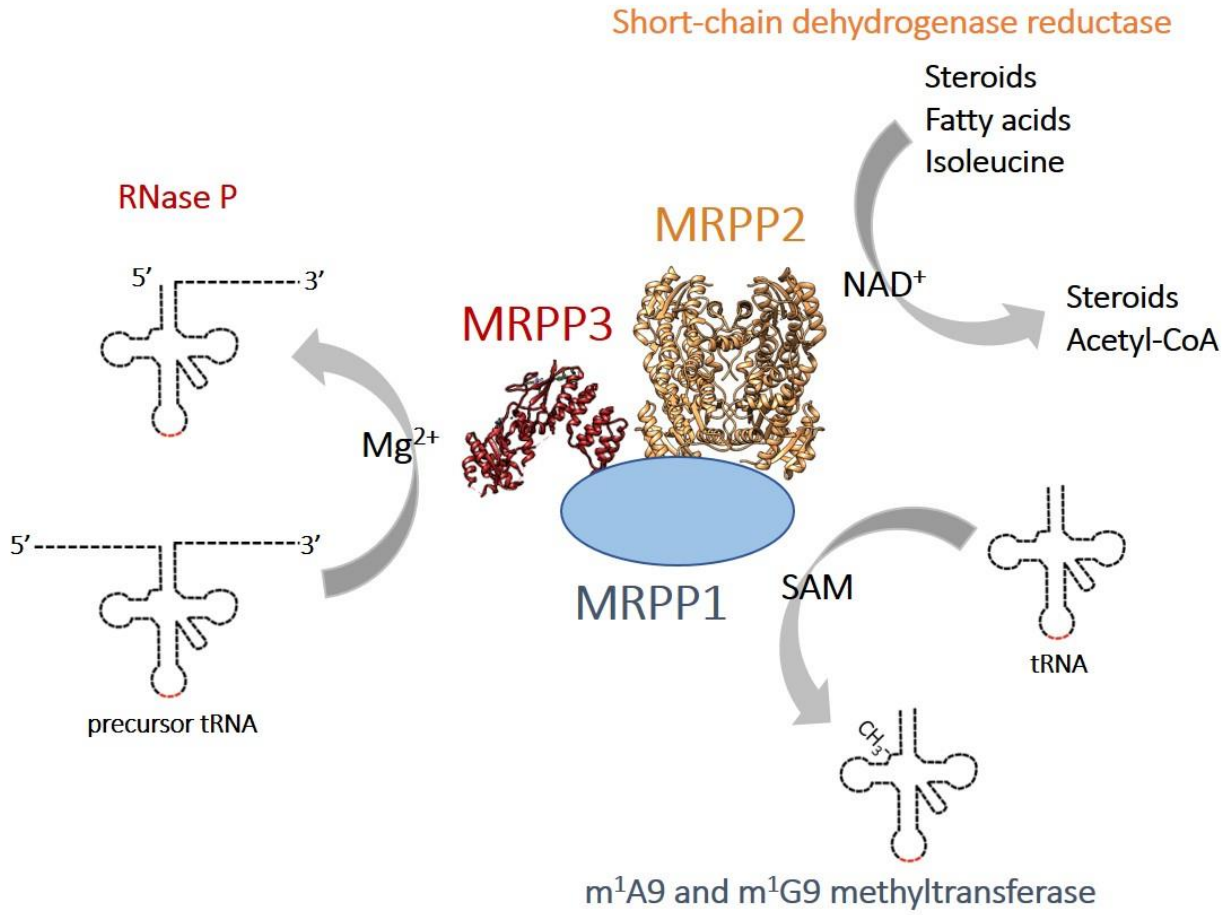

Highlights:

- Two novel missense mutations were identified in *HSD17B10* in two separate families.
- Both mutations lowered residual dehydrogenase activity of HSD10 *in vivo*.
- The mutant proteins disrupted all HSD10-associated activities differently *in vitro*.
- One mutation (p.V12L) reduced protein stability *in vitro*.
- The other mutation (p.V176M) impaired kinetics and complex formation *in vitro*.